Lithium and phosphorus-functionalized graphitic carbon nitride monolayer for efficient hydrogen storage: A DFT study

Deepak Kumar Gorai (Deepakrai@iitkgp.ac.in)
Indian Institute of Technology Kharagpur

Tarun Kumar Kundu
Indian Institute of Technology Kharagpur

Research Article

Keywords: Density functional theory, g-C3N4 monolayer, Co-doping, Hydrogen adsorption

Posted Date: November 10th, 2022

DOI: https://doi.org/10.21203/rs.3.rs-2242792/v1

Abstract

We have explored the consequence of lithium and phosphorous functionalization on the graphitic carbon nitride (g-C_3N_4) monolayer for hydrogen storage using density functional theory. Both pristine and Li and P decorated g-C_3N_4 show a semiconductor nature. The substantial overlap between the *s* orbital of Li and the *p* orbital of nitrogen near the Fermi level shows the binding between Li and the g-C_3N_4. The repositioning of HOMO and LUMO is noticed in the Li and P decorated g-C_3N_4. The Bader charge analysis indicates the charge allocation from the Li and P atom to the g-C_3N_4, which results in the adsorption of H_2 by electrostatic interaction. The hydrogen storage capacity of 5.78 wt% is obtained after functionalizing Li and P into the g-C_3N_4. The obtained adsorption energies for the H_2 adsorption confirm that Li and P functionalized g-C_3N_4 is a mesmerizing candidate for the reversible loading of H_2 at ambient conditions.

1. Introduction

Hydrogen is considered a promising candidate to encounter energy necessity since it is a clean, nontoxic, economical, abundant, environment-friendly, and renewable energy source [1–3]. Numerous hydrogen storage mechanisms have been projected in the last decades via the physisorption and chemisorption processes to discover suitable material [4–6]. The U.S Department of Energy (DOE) system has fixed a target of 5.5 wt% gravimetric hydrogen storage capacity and 0.05 Kg hydrogen/L volumetric capacity for onboard light-duty vehicles, materials-handling equipment, and moveable power applications by the end of 2025 [7]. Nevertheless, developing materials that can accumulate hydrogen by that standard and function under ambient conditions is not easy.

The hydrogen bonding is either too feeble when interacting with carbon nanostructure or too robust as inorganic molecules and light metal hydrides [8, 9]. So, continuous efforts are given to find the ideal storage system with binding energy intermediate between physisorption and chemisorption. Formerly, $LiBH_4$ has been considered a suitable material due to its 18.4 wt% hydrogen storage capacity, but this hybrid assembly is comparatively unbalanced at high temperatures (400^oC) [10]. Recently, nanostructures based on carbon and graphene have been recommended for hydrogen loading claims as a result of their excellent surface-to-volume ratio, porous structure, and lightweight. Zhang et al. have reported in theory that graphitic carbon nitride (g-C_3N_4) (triazine-based) is an admirable material for the steady and sound-dispersed embellishment of Ti atoms with high hydrogen adsorption capacity and binding strength appropriate for mobile application [11]. M.D. Ganji et al. have studied the hydrogen storage capacity of Si-decorated graphene sheets using density functional theory (DFT) and found ~ 15 wt% of hydrogen storage capacity by considering hydrogen on both sides of the Si-decorated graphene sheet [12]. Menghao Wu et al. have found that Li-functionalization on g-C_3N_4 has a large capacity of 10 wt% for hydrogen storage [13]. Also, Y. Wang et al. have shown that g-C_3N_4 nanotubes functionalized with Na and Li atoms have a storage capacity of 9.09 wt% at 0 K for hydrogen [14]. Nevertheless, the binding strength of Li on the g-C_3N_4 has been computed to be just 2.20 eV at 0 K, which would encourage the development of the Li-clusters at advanced process temperature and afterward reduce hydrogen storage capacity. Y. Liu et al. have found that up to 7.8 wt% of H_2 molecules can be stored by Ti-decorated graphene [15]. N. Song et al. have stated that up to 7.6 wt% of H_2 molecules can be stored with Ti-decorated boron-carbon-nitride [16].

Most theoretical studies on hydrogen storage are in triazine-based carbon nitride, even though the allotrope heptazine-based g-C_3N_4 is more stable and readily available for experimental studies. Wu et al. have found that Li-functionalized heptazine-based g-C_3N_4 is a hopeful material for H_2 storage [13]. Hussain et al. have extended the

work done by Wu et al. by using dispersion corrections and considering large supercells in the DFT calculations [17]. They find out the effect of different Li decorations on the storage capacity of heptazine-based g-C_3N_4 for H_2 storage. Our recent work demonstrated that P doping as distinct and organized with metal outcomes in sturdy delocalization of frontier molecular orbitals (MOs), which slows and opposes the charge recombination rate in the g-C_3N_4 [18]. The P doping in g-C_3N_4 changes the electronic structure of g-C_3N_4 with lesser bandgap energy and boosts electric conductivity and dye degradation capacity [19, 20]. Thus, in this work, we have investigated the synergetic consequence of lithium and phosphorus decoration on the structural, electronic, and optical properties and hydrogen storage capacity of the heptazine-based g-C_3N_4 monolayer.

2. Computational Methods

The density functional theory-based calculations are made in MedeA-VASP (Vienna Ab Initio Simulation Package) with the projector augmented-wave pseudopotential and PBE-GGA functional [21, 22]. A supercell of the g-C_3N_4 layer with a 2 × 2 × 1 unit cell size [(g-C_3N_4)$_8$] is used in all the calculations. A vacuum space of 18 Å is kept between head-to-head layers to avoid interactions between them, and 3 × 3 × 1 k-points and 500 eV cut-off energy is chosen for the structure optimization. 5 × 5 × 1 k-points mesh is considered for the density of states (DOS) and band structure calculations. The cut-off criteria for energy and force convergence are kept at 1 × 10^{-5} eV and 0.05 eV/ Å, respectively. The van der Walls (vdW) interactions are computed with the help of Tkatchenko and Scheffer (T.S.) correction [23]. The Monkhorst-Pack arrangement is used to sample the Brillouin zone. The value of Gaussian smearing width is seized to be 0.2. The Bader charge study approaches the allocation of electronic charge among Li, P dopants, adsorbed hydrogen, and the monolayer [24].

The interaction energy of the Li and P dopants on the g-C_3N_4 monolayer is calculated as [25]:

$$E_{int}(Li/P) = \{E\left(Li_mP_n(g-C_3N_4)_8\right) - E\left((g-C_3N_4)_8\right) - mE\left(Li\right) - nE\left(P\right)\}/(m+n)$$

1

where m and n are the quantity of added Li and P atoms, respectively. *E(X)* is the energy of the composite, molecule, or atom, *X*. A favorable interaction is given by the negative interaction energy.

The H_2 adsorption energy E_{ads} (xH_2) of the Li and P functionalized systems is computed using the:

$$E_{ads}\left(xH_2\right) = E\left(xH_2Li_mP_n(g-C_3N_4)_8\right) - E\left(Li_mP_n(g-C_3N_4)_8\right) - xE\left(H_2\right)$$

2

The adsorption energy per H_2 molecule (E_{ads}/H_2) is calculated using the equation below:

$$E_{ads}/H_2 = \left[E_{ads}\left(xH_2\right)\right]/\left(x\right)$$

3

Where *x* is the quantity of adsorbed H_2 molecules, the negative value of adsorption energy indicates energetically favorable adherence.

Further, the charge density difference (CDD) is computed using the following formula:

$$\Delta\rho = \rho_{(adsorbedstate)} - \rho_{(adsorbent)} - \rho_{(substrate)}$$

4

where $\rho_{(adsorbedstate)}$ and $\rho_{(substrate)}$, represent the total electron densities of the monolayer with and without adsorbed H_2, respectively, and $\rho_{(adsorbent)}$ represent the total electron density of the secluded H_2 molecule.

The total electron density plots and the charge density difference plots are obtained using VESTA 3.5.7 software [26]. The PBE0 [27] functional and the Lanl2dz [28] basis set are used for the frontier MOs estimation in Gaussian 16 software [29].

To study the optical properties of pristine and metals embedded g-C_3N_4 systems, optical absorption ($\alpha(\omega)$) and optical conductivity ($\sigma_1(\omega)$) are calculated using the following formulae [30]:

$$\alpha(\omega) = \sqrt{2}\omega\sqrt{\sqrt{{}_1(\omega)^2 + {}_2(\omega)^2} - {}_1(\omega)}$$

5

$$\sigma_1(\omega) = \left(\omega\ {}_2(\omega)\right)/4\pi$$

6

Where ω is the light frequency, ${}_1(\omega)$ and ${}_2(\omega)$ are the real and imaginary fragments of dielectric function correspondingly.

3. Results And Discussions

3.1 Li and P functionalization on g-C_3N_4

The optimized structure of pristine g-C_3N_4 monolayer is shown in Fig. 1(a), and a cell constant value of a = 7.134 Å = b is obtained, which is consistent with previously simulated (7.14 Å) as well as experimental (6.810 Å) outcomes [31, 32]. According to the symmetry of the g-C_3N_4, there are two distinct carbon atoms (C1 and C2) and three distinct nitrogen atoms (N1, N2, and N3) (Fig. 1a) [33]. There are five substitutional sites (C1, C2, N1, N2, and N3) and two interstitial sites (I1 and I2), as shown in Fig. 1(a), for the loading of metals and non-metals in heptazine-based g-C_3N_4 [18]. The large cavity (I2 site) is the steadiest position for metal loading, and the P atom at I1/I2 site is the most reliable configuration compared to other doping sites [34, 35]. Therefore, we have considered a large cavity for the Li atom and the I1 site for the P atom. In the case of single Li atom adsorption on the g-C_3N_4 monolayer, the Li atom is positioned in the center of the membrane plane's pore, with the adsorption energy of − 4.36 eV, very close to the result reported in the literature [36]. However, three Li in the large pore orient directly above (2.04 Å above the monolayer plane) the cavity with a slight shift of internal nitrogen towards the Li atoms after optimization (Fig. 1(c)) with adsorption energy of -3.61 eV [37]. The adsorption energy (E_{ads} = -3.61 eV) of Li on the g-C_3N_4 monolayer is considerably more than the cohesive energy (E_{coh} = -1.63 eV) of Li [13]. This adsorption energy value shows an even dispersal of Li dopants without cluster formation. As shown in Fig. 1(c), the length between the Li atom and the adjacent N atoms is ~ 1.89 Å, while the distance between two Li atoms is about 3.52 Å. In the case of Li and P functionalized g-C_3N_4, we have considered a g-C_3N_4 monolayer having three Li atoms and one P atom in the empty

cavity at a distance of 2 Å from the monolayer plane. After the geometry optimization, the P atom sits 2.37 Å above the monolayer plane, and the space between the P and the neighboring C and N atoms are 1.79 Å and 1.83 Å, respectively, as shown in Fig. 1(d). The high adsorption energy value (-3.94 eV) ensures the stability of the Li and P functionalized g-C_3N_4 monolayer. This configuration is carefully chosen to guarantee judicious space for the adsorption of H_2 all over the Li and P on the two sides of the monolayer.

The electronic band structure, along with the partial density of states (PDOS), is also used to study the functionalization of Li and P into the g-C_3N_4 monolayer. The band structure indicates the semiconducting nature of the g-C_3N_4 monolayer having a bandgap of 1.1 eV (Fig. 2(a)), which is less than the reported experimental value of 2.7 eV due to the well-identified fact that GGA-PBE underrates the bandgap energy [38]. Nonetheless, while the band gap calculated from GGA-PBE is not close to the experimental value, it gives vital insight into the impacts of element doping on g-C_3N_4, particularly on partial DOS, projected DOS, electronic band structure, and optical properties [39, 40]. Hence, as discussed in the manuscript, we have used GGA-PBE to calculate the properties of all the doped systems. After the Li addition to the g-C_3N_4 monolayer, the band structure changes significantly due to the allocation of extra electrons from the Li to N, causing the Li-doped g-C_3N_4 monolayer to become metallic [37]. After adding Li and P to the g-C_3N_4 monolayer, its metallic nature diminishes with a feeble bandgap of 0.036 eV, as shown in Fig. 2(c). The partial density of states (PDOS) of valence *s* orbital of the Li atom and *p* orbital of P, C, and N atoms (close to the Li and P atoms) are shown in Fig. 2(d)-(f). In a pure g-C_3N_4 monolayer, the valence band is principally contributed by the *2p* orbital of the N atom, while the conduction band is conquered by the *2p* orbital of the C atom (Fig. 2(d)). Over the incorporation of Li atoms in the g-C_3N_4 monolayer, mid-band states appear near the Fermi level due to the transfer of additional electrons from Li to N, as revealed in Fig. 2(e). The binding of Li to the monolayer is indicated by the substantial overlap between the *2s* orbital of Li and the *2p* orbital of N near the Fermi level. A similar trend can also be observed in the PDOS of Li and P added g-C_3N_4 monolayer, as visible in Fig. 2(f).

The frontiers MOs of the pristine-$(g\text{-}C_3N_4)_8$, $(g\text{-}C_3N_4)_8Li_3$, and $(g\text{-}C_3N_4)_8Li_3P$ monolayers are given in Fig. 3 to show the charge localization and delocalization. In the pristine g-C_3N_4 monolayer, there is a localization of photogenerated e^-/h^+ couples in a specific heptazine unit, which results in an extreme recombination proportion of e^-/h^+ couples. This charge localization explains the poor photocatalytic performance of pristine g-C_3N_4. In $(g\text{-}C_3N_4)_8Li_3$ and $(g\text{-}C_3N_4)_8Li_3P$ monolayers repositioning of HOMO and LUMO is observed, which indicates the delocalization of photogenerated e^-/h^+ pairs. This delocalization of e^-/h^+ pairs in the Li and P functionalized g-C_3N_4 monolayers result in the high photocatalytic performance related to the pristine g-C_3N_4 monolayer.

Next, we have calculated the electron localization function (ELF) plots of the pristine-$(g\text{-}C_3N_4)_8$, $(g\text{-}C_3N_4)_8Li_3$, and $(g\text{-}C_3N_4)_8Li_3P$ monolayers as shown in Fig. 1(b) and Fig. S2. It has been noticed from the ELF plots that the C-N bonds are covalent, while Li-N and P-N are ionic.

As displayed in Fig. 4, we have also calculated the optical properties, for example, refractive index, reflectivity, optical conductivity, and optical absorption of pure, Li functionalized, and Li and P functionalized graphitic carbon nitride. There is a substantial perfection in the reflectivity in the infrared area after adding Li and P atoms to the pure graphitic carbon nitride, as revealed in Fig. 4(b). Optical conductivity is considered a crucial means for studying electronic circumstances in materials. Figure 4(c) shows robust growth in the optical conductivity in the infrared as well as visible area after adding Li and P atoms. Li-functionalized graphitic carbon nitride shows better optical absorption in the infrared region. However, Li and P functionalized graphitic carbon nitride has the best absorption in

the visible and ultraviolet region compared to pristine as well as Li functionalized g-C_3N_4 monolayers, as shown in Fig. 4(d).

3.2 Adsorption of H_2 on the Li and P decorated g-C_3N_4 monolayer

After confirming the stability of Li and P functionalized graphitic carbon nitride monolayer, we have explored the interaction of the H_2 molecule with Li and P decorated g-C_3N_4 monolayer by placing H_2 molecules over Li and P atoms in the supercell. The optimized structures of different configurations of Li and P functionalized graphitic carbon nitride with the maximum quantity of H_2 adsorbed only on one side of the monolayer are given in Fig. 5. After geometry optimization, the adsorption energy, bond length, average Li-H_2 distance, and average P-H_2 distance are noted in Table 1. At first, a single H_2 molecule is placed near the individual Li and P atoms, and the structure is optimized. We progressively increase the quantity of H_2 molecules, and the structure is re-optimized after each H_2 molecule addition (Fig. 5(d), Fig. 5(e), and Fig. 5(f)). It is found that the highest number of H_2 adsorbed per Li and P atoms in the instance of $(g\text{-}C_3N_4)_8Li_3P$ is three, as shown in Fig. 5(f); the fourth H_2 is kept away from the monolayers. A reasonable fraction of the distance is preserved between the H_2 molecules to bypass annoying repulsions.

The adsorption energy of the first H_2 molecule is evaluated using Eq. 2 and is come up with − 0.131 eV considering GGA-vdW for $(g\text{-}C_3N_4)_8Li_3P$ (Fig. 5(d)). For the second and the third H_2 molecule, the adsorption energies are − 0.093 and − 0.089 eV, respectively, for $(g\text{-}C_3N_4)_8Li_3P$. Even more importantly, according to Table I, the adsorption energies are doubled upon, including dispersion corrections. Hence van der Waals forces play a significant role in the binding. Also, as given in Table 1, the adsorption energies reduce thru the rise of H_2, suggesting that the system can adsorb an inadequate amount of H_2. It has been noticed that the distance between two hydrogen atoms (H-H) is elongated than the isolated H_2 (0.75 Å). This elongation is due to the polarization between the Li, P, and H_2, as shown in Table 1.

Further, it is observed that the average Li-H_2 and P-H_2 distances increase with the intensification of adsorbed H_2; however, the H-H bond length shrinkages. This decrease in the H-H bond span implies that the adsorption strength decreases with the intensification of the adsorbed H_2. This is confirmed by the adsorption energies of different configurations, as given in Table 1. It is observed that the computed adsorption energy is diminished from − 0.131 eV for single adsorbed H_2 to -0.065 eV per H_2 for the six adsorbed H_2 on the Li and P functionalized g-C_3N_4, which may be attributable to the steric repulsion between the adsorbed H_2 molecules [14]. Even though the typical adsorption energy for each H_2 decreases as the quantity of H_2 increases, the adsorption energy for each H_2 is typical for solid physisorption in the six H_2 adsorbed Li and P functionalized g-C_3N_4 [12].

Table 1
The adsorption energy for each H_2 (GGA, GGA + vdW), average Li-H_2 distances, average P-H_2 distances, and typical H-H bond lengths on Li and P decorated carbon nitride monolayers.

System	Total Adsorption energy [E_{ads} (H_2) in eV]	Adsorption energy per H_2 [E_{ads} /H_2 in eV]		Li – H_2 distance (Å)	P – H_2 distance (Å)	H – H bond length (Å)
	GGA + vdW	GGA	GGA + vdW			
$(g\text{-}C_3N_4)_8Li_3$ + $3H_2$	-0.363	-0.059	-0.121	2.07	-	0.756
$(g\text{-}C_3N_4)_8Li_3$ + $6H_2$	-0.642	-0.056	-0.107	2.28	-	0.755
$(g\text{-}C_3N_4)_8Li_3$ + $9H_2$	-0.945	-0.045	-0.105	2.66	-	0.752
$(g\text{-}C_3N_4)_8Li_3P$ + $4H_2$	-0.524	-0.082	-0.131	2.18	3.07	0.759
$(g\text{-}C_3N_4)_8Li_3P$ + $8H_2$	-0.744	-0.043	-0.093	2.22	3.08	0.757
$(g\text{-}C_3N_4)_8Li_3P$+$12H_2$	-1.068	-0.037	-0.089	2.27	3.20	0.754
$(g\text{-}C_3N_4)_8Li_3P$+$16H_2$	-2.128	-0.080	-0.133	2.30	3.34	0.754
$(g\text{-}C_3N_4)_8Li_3P$+$20H_2$	-1.740	-0.043	-0.087	2.32	3.42	0.752
$(g\text{-}C_3N_4)_8Li_3P$ + $24H_2$	-1.560	-0.034	-0.065	2.33	3.50	0.751

The graph of volumetric capacity vs. gravimetric capacity is shown in Fig. 7. The ultimate H_2 storage capacity of $(g\text{-}C_3N_4)_8Li_3$ (Fig. 5(c)) and $(g\text{-}C_3N_4)_8Li_3P$ (Fig. 5(f)) are found 2.34 ($9H_2$) and 2.98 wt % ($12H_2$) respectively, with the adsorption of H_2 to just a single side of the monolayer. Finally, we have allowed the adsorption of H_2 on both sides of the monolayers (Fig. 6). By the adsorption of H_2 on both sides, we have obtained a gravimetric and volumetric capacity of 5.78 wt% hydrogen and 0.0275 Kg hydrogen/L, respectively, for the $(g\text{-}C_3N_4)_8Li_3P$ configuration (Fig. 7). These values are pretty close to the U.S. Department of Energy (DOE) [7].

3.3 Nature of interaction between H_2 and Li and P functionalized $g\text{-}C_3N_4$ monolayer

To determine the nature of the Li and P functionalization binding on the $g\text{-}C_3N_4$ monolayer and the adsorption of hydrogen molecules on the Li and P functionalized $g\text{-}C_3N_4$ monolayer qualitatively, we have plotted the total electron density. Here is no electron density at the interface area between the Li atom and $g\text{-}C_3N_4$ monolayer and amid H_2 and the Li atom (Fig. 8 (a) and (b)). These electron density plots specify that the Li functionalization on the $g\text{-}C_3N_4$ and the H_2 adsorption on the Li functionalized $g\text{-}C_3N_4$ do not form a covalent bond along the $g\text{-}C_3N_4$, indicating the

physical nature of the adsorption. The same type of bonding nature is also observed in the case of Li and P functionalization on the g-C_3N_4 monolayer, as shown in Fig. 8 (c) and (d), which is also confirmed previously by the adsorption energy calculation as given in Table 1.

The CDD plots of the systems, as mentioned earlier, are shown in Fig. 9. As can be seen from Fig. 9 (a) and Fig. 9 (c), few charges exit on the topmost of Li and P atoms, while most of the charges are mainly concentrated near the g-C_3N_4 monolayer, which indicates some charges transfer from Li and P atoms to the g-C_3N_4 monolayer. These partially charged Li (P) ions and the g-C_3N_4 monolayer would yield a local electric field. These local electric fields polarized the hydrogen molecules and bound them thru the polarization phenomenon [41]. Hence the H_2 gets polarized with the electron density gathering on the side adjacent to the g-C_3N_4 monolayer and the depletion on the side, aside from the g-C_3N_4 monolayer, as shown in Fig. 9 (b) and Fig. 9 (d). This polarization is the reason behind the elongation of the H-H bond in the H_2 adsorbed on the Li and P functionalized g-C_3N_4 compared to the H-H bond in the isolated H_2. Hence, we can say that the H_2 adsorption on the Li and P functionalized g-C_3N_4 features dipole-dipole interactions [14].

We have calculated the charge transfer by Bader charge analysis as given in Table 2 [42]. Individual Li drops nearly 0.90 $\mathbf{e}^-$ to the monolayer in Li atoms added g-C_3N_4 monolayer, while each Li atom loses almost 0.90 $\mathbf{e}^-$ and the P atom loses approximately 0.80 $\mathbf{e}^-$ in case of Li and P atoms added g-C_3N_4 monolayer. This charge transfer suggests that the bonding between Li and g-C_3N_4 monolayer and between P and g-C_3N_4 monolayer is ionic, proved previously by the ELF plots as shown in Fig. S2. These + ve charged Li and P ions yield local electric fields that polarize H_2 molecules and thus enhance the adsorption [43,44]. Hence, finding a system in which the metal ion is remained positively charged is the key to molecular hydrogen adsorption [45]. Since no charge transfer takes place in the case of the physisorption mechanism, the amount of hydrogen that can be stored on the Li and P functionalized g-C_3N_4 monolayer is limited mainly by steric hindrance.

Table 2
Bader charges of C and N atoms before and after Li and P functionalization and H_2 adsorption.

Configuration	Bader charges (e^-)												
	Before (Li/P) functionalization				After (Li/P) functionalization				After H_2 adsorption				
	C	N	Li	P	C	N	Li	P	C	N	Li	P	H
$(g\text{-}C_3N_4)_8Li_3$	1.56	-1.17	-	-	1.45	-1.16	0.80	-	1.44	-1.16	0.79	-	-0.003
$(g\text{-}C_3N_4)_8Li_3P$	1.56	-1.17	-	-	1.30	-1.17	0.80	0.90	1.31	-1.17	0.89	0.79	-0.004

To understand the nature of the H_2 adsorption on the Li and P functionalized g-C_3N_4, we have plotted the densities of states for the hydrogen molecule, Li atoms, P atom, and the g-C_3N_4 of the H_2 adsorbed Li and P functionalized g-C_3N_4. The Fermi level is fixed to zero in these plots. As shown in Fig. 6(d), there is no apparent hybridization between the Li and P functionalized g-C_3N_4 monolayer and the adsorbed hydrogen molecule. Therefore, the hydrogen adsorption mechanism in Li and P functionalized g-C_3N_4 monolayer is reasonably different from the Kubas interaction, which generally occurs in transition metal-doped materials [46]. In Kubas interaction, stronger hybridization exists between the *d* orbital of the functionalized transition metal and the adsorbed hydrogen σ orbital.

4. Conclusion

Density functional theory-based calculations are performed to examine the outcome of lithium and phosphorus decoration on the structural, electronic, and optical properties and the hydrogen storage capacity of the heptazine-based g-C_3N_4 monolayer. Band structure calculation indicates that graphitic carbon nitride is a semiconductor that becomes conducting after adding Li and almost loses its metallic nature after adding both Li and P. The interaction of Li to the monolayer is indicated by the substantial overlap between the *2s* orbital of Li and the *2p* orbital of N near the Fermi level with the help of PDOS. The frontiers MOs calculation shows the repositioning of HOMO and LUMO in the Li and P decorated g-C_3N_4. The Bader charge investigation has disclosed the presence of Li and P cations owing to the charge allocation from the Li and P atoms to the monolayer. These cations provide the site for the adsorption of hydrogen molecules via electrostatic interaction and van der Waals interaction. The utmost hydrogen storage capacity of 5.78 wt% is obtained by carefully functionalizing Li and P atoms into the g-C_3N_4. The obtained values of H_2 adsorption energies designate that Li and P functionalized g-C_3N_4 is a fascinating candidate for the alterable loading of H_2.

Declarations

Ethical approval

'Not applicable'

Competing Interest

The authors declare that they have no known competing financial interests or personal relationships that could have appeared to influence the work reported in this paper.

Authors' contributions

Deepak Kumar Gorai (author 1): Conceptualization, DFT calculations, analyses, and article writing; **Tarun Kumar Kundu** (author 2): Computational resources, supervision, editing, and manuscript review.

Funding

The author(s) received no financial support for this article's research, authorship, and/or publication.

Availability of data and materials

The datasets generated during and/or analyzed during the current study are available from the corresponding author on reasonable request.

Acknowledgment

The authors would like to gratify the Ministry of Human Resource Development (MHRD), Govt. of India, for the fellowship assistantship and the Indian Institute of Technology, Kharagpur, India, 721302, for providing the computational facilities required for the present work. The authors also acknowledge the National Supercomputing Mission (NSM) for providing computing resources of 'PARAM Shakti' at IIT Kharagpur, which is implemented by C-DAC and supported by the Ministry of Electronics and Information Technology (MeitY) and Department of Science and Technology (DST), Government of India.

References

1. Jena, P., 2011. Materials for hydrogen storage: past, present, and future. *The Journal of Physical Chemistry Letters*, *2*(3), pp.206-211.
2. Turner, J.A., 2004. Sustainable hydrogen production. *Science*, *305*(5686), pp.972-974.
3. Züttel, A., 2003. Materials for hydrogen storage. *Materials Today*, *6*(9), pp.24-33.
4. Nikitin, A., Li, X., Zhang, Z., Ogasawara, H., Dai, H., and Nilsson, A., 2008. Hydrogen storage in carbon nanotubes through the formation of stable C− H bonds. *Nano Letters*, *8*(1), pp.162-167.
5. Pistidda, C., Bergemann, N., Wurr, J., Rzeszutek, A., Møller, K.T., Hansen, B.R., Garroni, S., Horstmann, C., Milanese, C., Girella, A. and Metz, O., 2014. Hydrogen storage systems from waste Mg alloys. *Journal of power sources*, *270*, pp.554-563.
6. Zhang, W., Zhang, S., Zhang, Z., Wang, L., and Yang, W., 2014. The hydrogen adsorption on Zr-decorated LiB (001): A DFT study. *Vacuum*, *110*, pp.62-68.
7. U.S Department of Energy. Fuel cell technologies office multi-year research, development, and demonstration plan. 2020. URL, http://energy.gov/eere/fuelcells.
8. Voss, J., Shi, Q., Jacobsen, H.S., Zamponi, M., Lefmann, K. and Vegge, T., 2007. Hydrogen dynamics in Na_3AlH_6: a combined density functional theory and quasielastic neutron scattering study. *The Journal of Physical Chemistry B*, *111*(15), pp.3886-3892.
9. Yang, R.T., 2000. Hydrogen storage by alkali-doped carbon nanotubes revisited. *Carbon*, *38*(4), pp.623-626.
10. Schlapbach, L. and Züttel, A., 2011. Hydrogen-storage materials for mobile applications. In *Materials for sustainable energy: a collection of peer-reviewed research and review articles from nature publishing group* (pp. 265-270).
11. Zhang, Y., Sun, H. and Chen, C., 2009. New template for metal decoration and hydrogen adsorption on graphene-like C_3N_4. *Physics Letters A*, *373*(31), pp.2778-2781.
12. Ganji, M.D., Emami, S.N., Khosravi, A. and Abbasi, M., 2015. Si-decorated graphene: a promising media for molecular hydrogen storage. *Applied Surface Science*, *332*, pp.105-111.
13. Wu, M., Wang, Q., Sun, Q. and Jena, P., 2013. Functionalized graphitic carbon nitride for efficient energy storage. *The Journal of Physical Chemistry C*, *117*(12), pp.6055-6059.
14. Wang, Y.S., Li, M., Wang, F., Sun, Q. and Jia, Y., 2012. Li and Na Co-decorated carbon nitride nanotubes as promising new hydrogen storage media. *Physics Letters A*, *376*(4), pp.631-636.
15. Liu, Y., Ren, L., He, Y. and Cheng, H.P., 2010. Titanium-decorated graphene for high-capacity hydrogen storage studied by density functional simulations. *Journal of Physics: Condensed Matter*, *22*(44), pp.445301.
16. Song, N., Wang, Y., Sun, Q. and Jia, Y., 2012. First-principles study of hydrogen storage on Ti (Sc)-decorated boron-carbon-nitride sheet. *Applied surface science*, *263*, pp.182-186.
17. Hussain, T., Hankel, M. and Searles, D.J., 2016. Computational evaluation of lithium-functionalized carbon nitride (g-C_6N_8) monolayer as an efficient hydrogen storage material. *The Journal of Physical Chemistry C*, *120*(44), pp.25180-25188.
18. Gorai, D.K. and Kundu, T. K., 2020. Influence of Pt and P doping on the performance of g-C_3N_4 monolayer. *Materials and Manufacturing Processes*, *35*(6), pp.625-634.
19. Zhang, Y. and Antonietti, M., 2010. Photocurrent generation by polymeric carbon nitride solids: an initial step towards a novel photovoltaic system. *Chemistry–An Asian Journal*, *5*(6), pp.1307-1311.

20. Zhang, L., Chen, X., Guan, J., Jiang, Y., Hou, T. and Mu, X., 2013. Facile synthesis of phosphorus-doped graphitic carbon nitride polymers with enhanced visible-light photocatalytic activity. *Materials Research Bulletin*, *48*(9), pp.3485-3491.
21. Kresse, G. and Furthmüller, J., 1996. Efficient iterative schemes for ab initio total-energy calculations using a plane-wave basis set. *Physical Review B*, *54*(16), p.11169.
22. Blöchl, P E 1994, 'Projector augmented-wave method', *Physical Review B*, vol. 50, pp. 17953-79.
23. A. Tkatchenko, M. Scheffler, Accurate molecular van der Waals interactions from the ground-state electron density and free-atom reference data, Phys. Rev. Lett. 102 (2009) 073005.
24. Bader, R. F. W. Atoms in Molecules - A Quantum Theory; Oxford University Press: Oxford, 1990.
25. Gorai, D.K. and Kundu, T.K., 2021. First principle study of lithium and phosphorus co-doped graphitic carbon nitride as a nonlinear optical material. *Materials Today Communications*, *26*, p.101911.
26. Momma, K. and Izumi, F., 2011. VESTA 3 for three-dimensional visualization of crystal, volumetric, and morphology data. *Journal of applied crystallography*, *44*(6), pp.1272-1276.
27. Adamo, C. and Barone, V., 1999. Toward reliable density functional methods without adjustable parameters: The PBE0 model. *The Journal of chemical physics*, *110*(13), pp.6158-6170.
28. Hay, P.J. and Wadt, W.R., 1985. Ab initio effective core potentials for molecular calculations. Potentials for the transition metal atoms Sc to Hg. *The Journal of chemical physics*, *82*(1), pp.270-283.
29. Frisch, M.J., Trucks, G.W., Schlegel, H.B., Scuseria, G.E., Robb, M.A., Cheeseman, J.R., Scalmani, G., Barone, V., Petersson, G.A., Nakatsuji, H. and Li, X., 2016. Gaussian 16 revision a. 03. 2016; gaussian inc. *Wallingford CT*, *2*(4).
30. Gorai, D.K. and Kundu, T.K., 2021. Platinum-silicon doped graphitic carbon nitride: A first principle calculation. *Physica B: Condensed Matter*, p.413547.
31. Zhang, X., Zhao, M., Wang, A., Wang, X., and Du, A., 2013. Spin-polarization and ferromagnetism of graphitic carbon nitride materials. *Journal of Materials Chemistry C*, *1*(39), pp.6265-6270.
32. Wang, X., Maeda, K., Thomas, A., Takanabe, K., Xin, G., Carlsson, J.M., Domen, K. and Antonietti, M., 2009. A metal-free polymeric photocatalyst for hydrogen production from water under visible light. *Nature Materials*, *8*(1), pp.76-80.
33. Gorai, D.K. and Kundu, T.K., 2020. First Principle Study of Na and P Co-Doped Heptazine Based Monolayer g-C3N4. *Materials Science Forum* (Vol. 978, pp. 369-376). Trans Tech Publications Ltd.
34. Ma, X., Lv, Y., Xu, J., Liu, Y., Zhang, R., and Zhu, Y., 2012. A strategy of enhancing the photoactivity of g-C_3N_4 via doping of non-metal elements: a first-principles study. *The Journal of Physical Chemistry C*, *116*(44), pp.23485-23493.
35. Gao, G., Jiao, Y., Waclawik, E.R. and Du, A., 2016. Single-atom (Pd/Pt) supported on graphitic carbon nitride as an efficient photocatalyst for visible-light reduction of carbon dioxide. *Journal of the American Chemical Society*, *138*(19), pp.6292-6297.
36. Zhu, L., Ma, X.G., Liu, N., Xu, G.W. and Huang, C.Y., 2016. Band structure modulation and carrier transport process of g-C_3N_4 doped with alkali metals. *Acta Physico-Chimica Sinica*, *32*(10), pp.2488-2494.
37. Zhu, G., Lü, K., Sun, Q., Kawazoe, Y. and Jena, P., 2014. Lithium-doped triazine-based graphitic C_3N_4 sheet for hydrogen storage at ambient temperature. *Computational materials science*, *81*, pp.275-279.
38. Gorai, D.K. and Kundu, T.K., 2022. NO adsorption on the Os, Ir, and Pt embedded tri-s-triazine based graphitic carbon nitride: A DFT study. *Applied Surface Science*, p.153104.

39. Chen, H., Qu, Y., Sun, L., Peng, J. and Ding, J., 2019. Band structures and optical properties of Ag and Al co-doped ZnO by experimental and theoretic calculation. *Physica E: Low-dimensional Systems and Nanostructures*, *114*, p.113602.
40. Sikam, P., Moontragoon, P., Ikonic, Z., Kaewmaraya, T. and Thongbai, P., 2019. The study of structural, morphological and optical properties of (Al, Ga)-doped ZnO: DFT and experimental approaches. *Applied Surface Science*, *480*, pp.621-635.
41. Niu, J., Rao, B.K. and Jena, P., 1992. Binding of hydrogen molecules by a transition-metal ion. *Physical review letters*, *68*(15), p.2277.
42. Tang, W., Sanville, E., and Henkelman, G., 2009. A grid-based Bader analysis algorithm without lattice bias. *Journal of Physics: Condensed Matter*, *21*(8), p.084204.
43. Jiang, Z.P., Zhou, X., Sun, Q., Wang, Q. and Jena, P., 2010. Geometry, electronic properties, and hydrogen adsorption properties of Li_3N-based nanostructures. *The Journal of Physical Chemistry C*, *114*(45), pp.19202-19205.
44. Zhou, J., Wang, Q., Sun, Q. and Jena, P., 2011. Enhanced hydrogen storage on Li functionalized BC_3 nanotube. *The Journal of Physical Chemistry C*, *115*(13), pp.6136-6140.
45. Sun, Q., Jena, P., Wang, Q. and Marquez, M., 2006. First-principles study of hydrogen storage on $Li_{12}C_{60}$. *Journal of the American Chemical Society*, *128*(30), pp.9741-9745.
46. Anikina, E.V., Banerjee, A., Beskachko, V.P. and Ahuja, R., 2020. Influence of Kubas-type interaction of B–Ni codoped graphdiyne with hydrogen molecules on desorption temperature and storage efficiency. *Materials Today Energy*, *16*, p.100421.

Figures

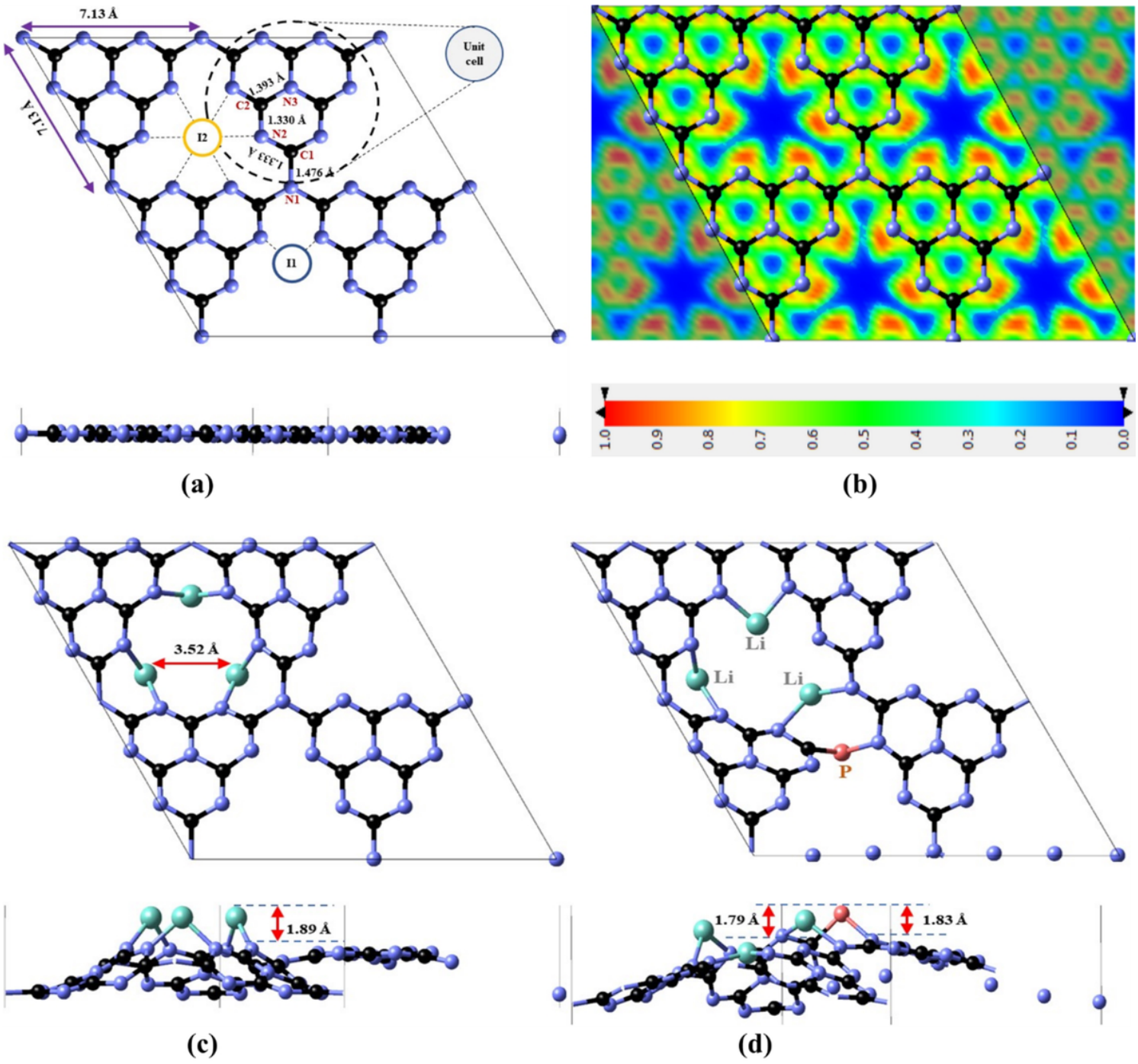

Figure 1

Top and side view of optimized structures of (a) pristine, (c) Li functionalized, (d) Li and P functionalized g-C_3N_4 monolayer, and (b) ELF plot of the pristine g-C_3N_4 monolayer.

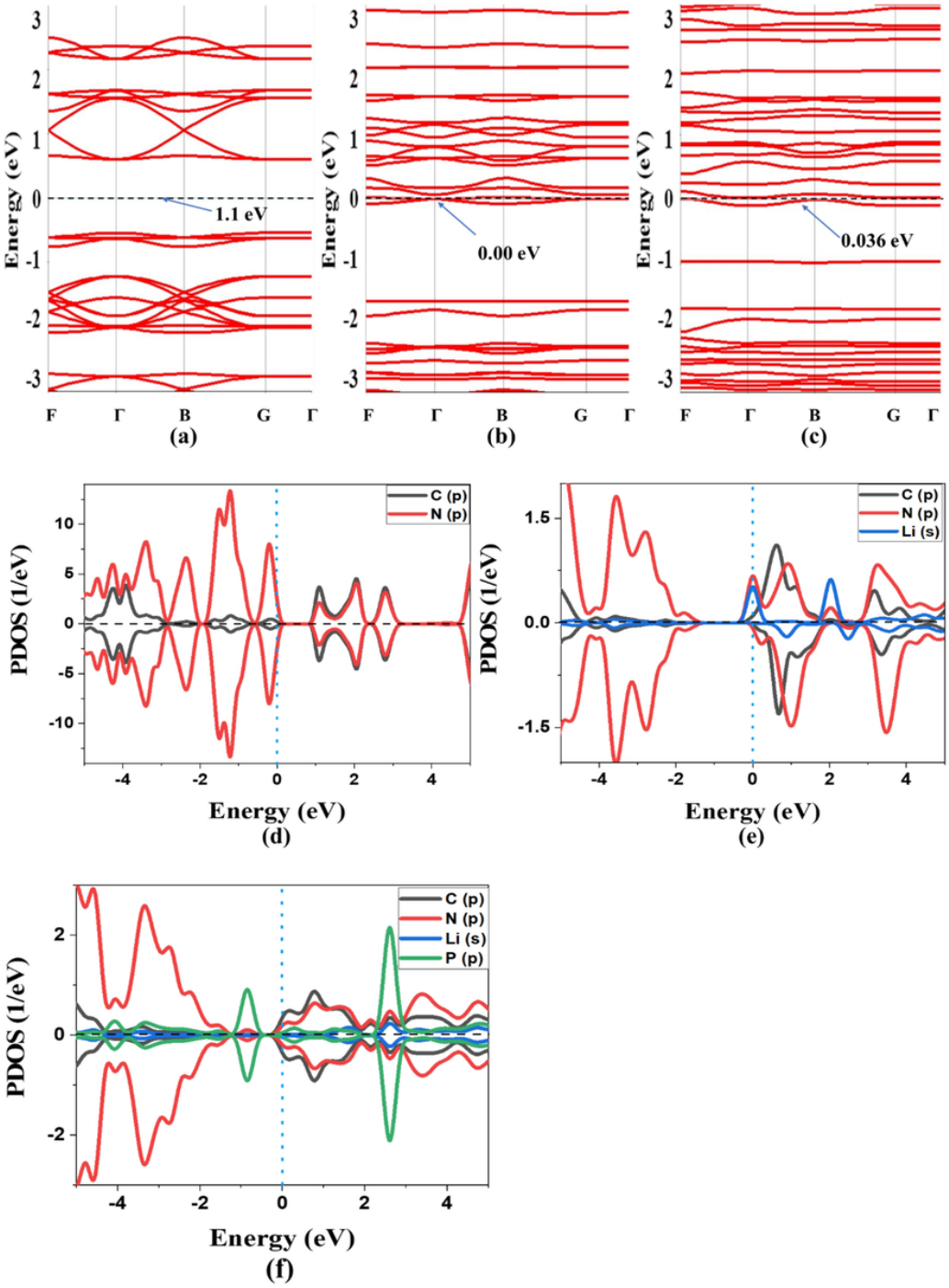

Figure 2

(a-c) Calculated band structures and (d-f) PDOS of the pristine-$(g\text{-}C_3N_4)_8$, $(g\text{-}C_3N_4)_8Li_3$, and $(g\text{-}C_3N_4)_8Li_3P$ monolayer, respectively.

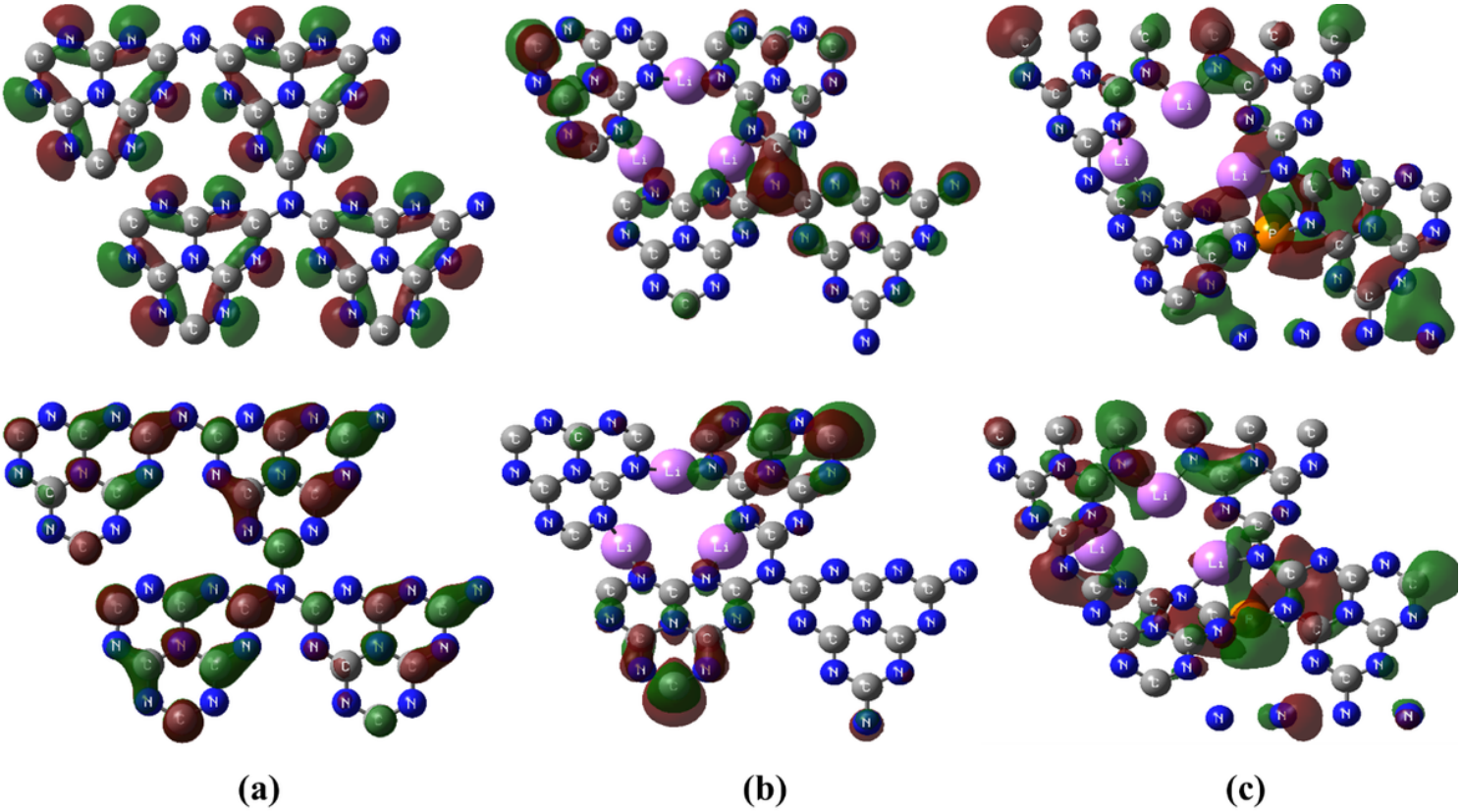

Figure 3

Calculated frontiers MOs [HOMO (top) and LUMO (bottom)] of the (a) pristine-$(g\text{-}C_3N_4)_8$, (b) $(g\text{-}C_3N_4)_8Li_3$, and (c) $(g\text{-}C_3N_4)_8Li_3P$ monolayer, respectively.

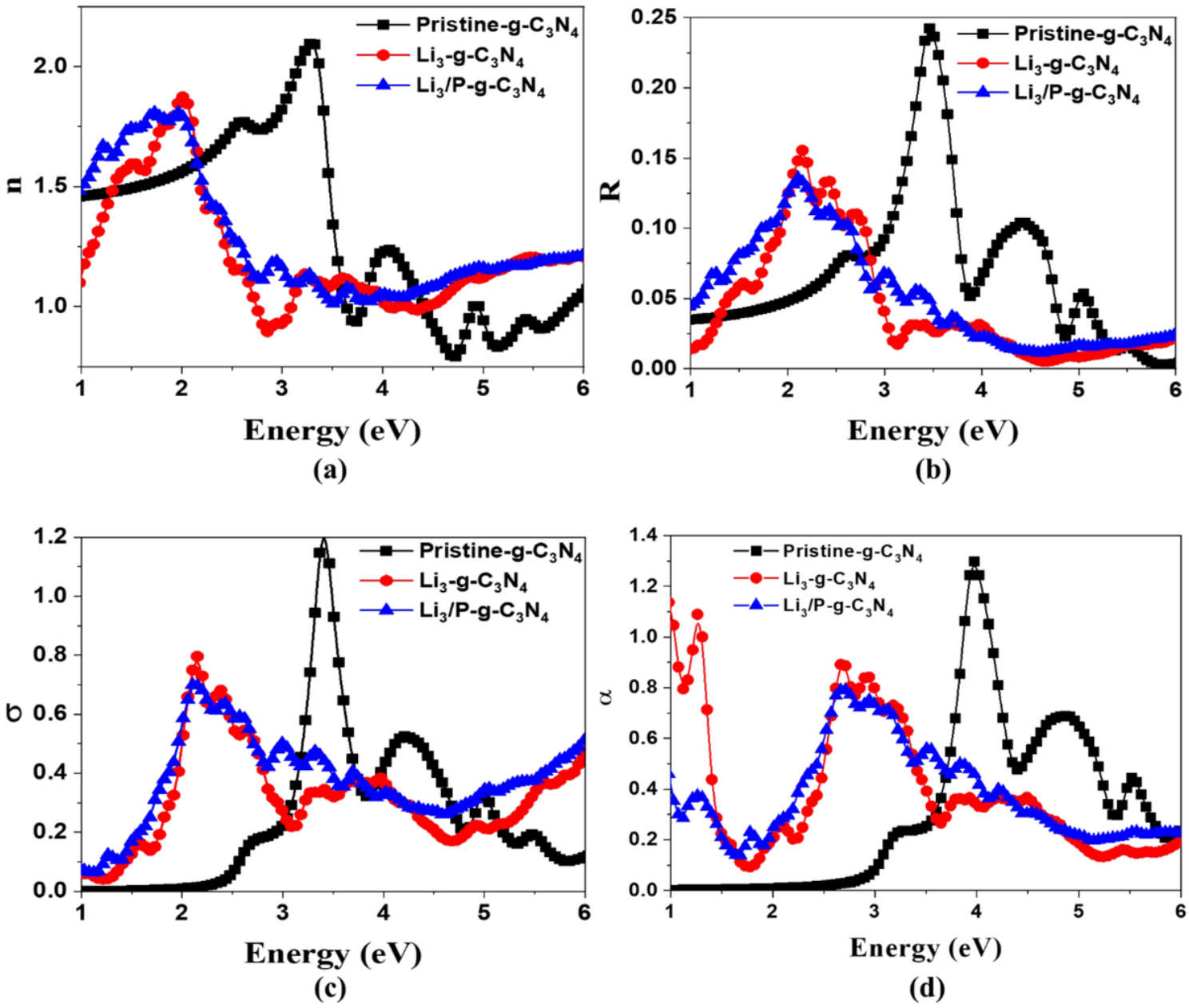

Figure 4

(a) Refractive index (n), (b) reflectivity (R), (c) optical conductivity (σ), and (d) optical absorption curve (α) of pristine, Li functionalized, and Li and P functionalized graphitic carbon nitride.

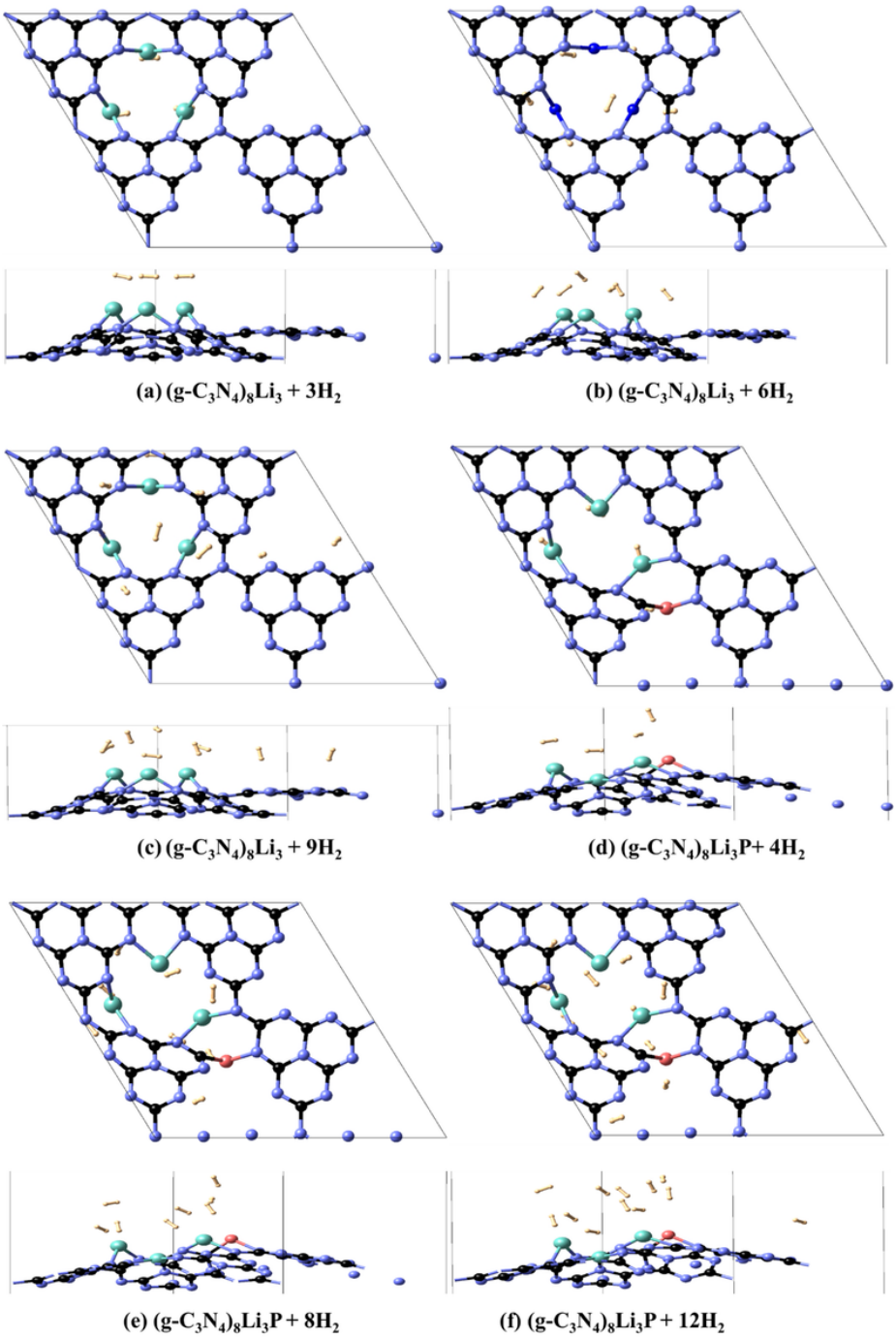

Figure 5

Different configurations of Li and P functionalized graphitic carbon nitride having three lithium atoms, a phosphorus atom, and H_2 molecules on the identical side of the monolayer.

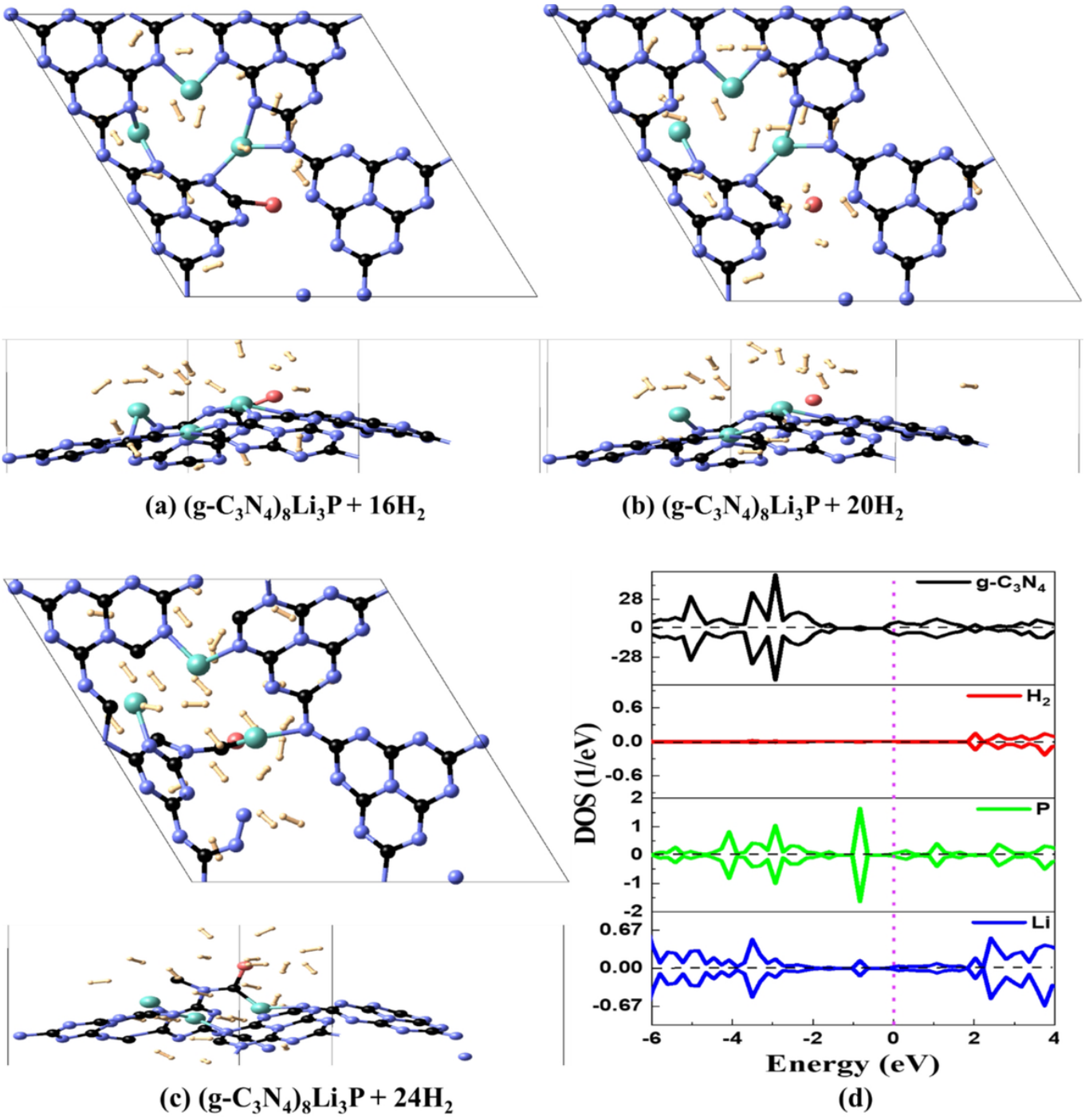

Figure 6

Different configurations of Li and P functionalized graphitic carbon nitride have three lithium atoms and a phosphorus atom on the same side of the monolayer, while H2 molecules are on both sides. (d) DOS plot of (g-$C_3N_4)_8Li_3P + 4H_2$.

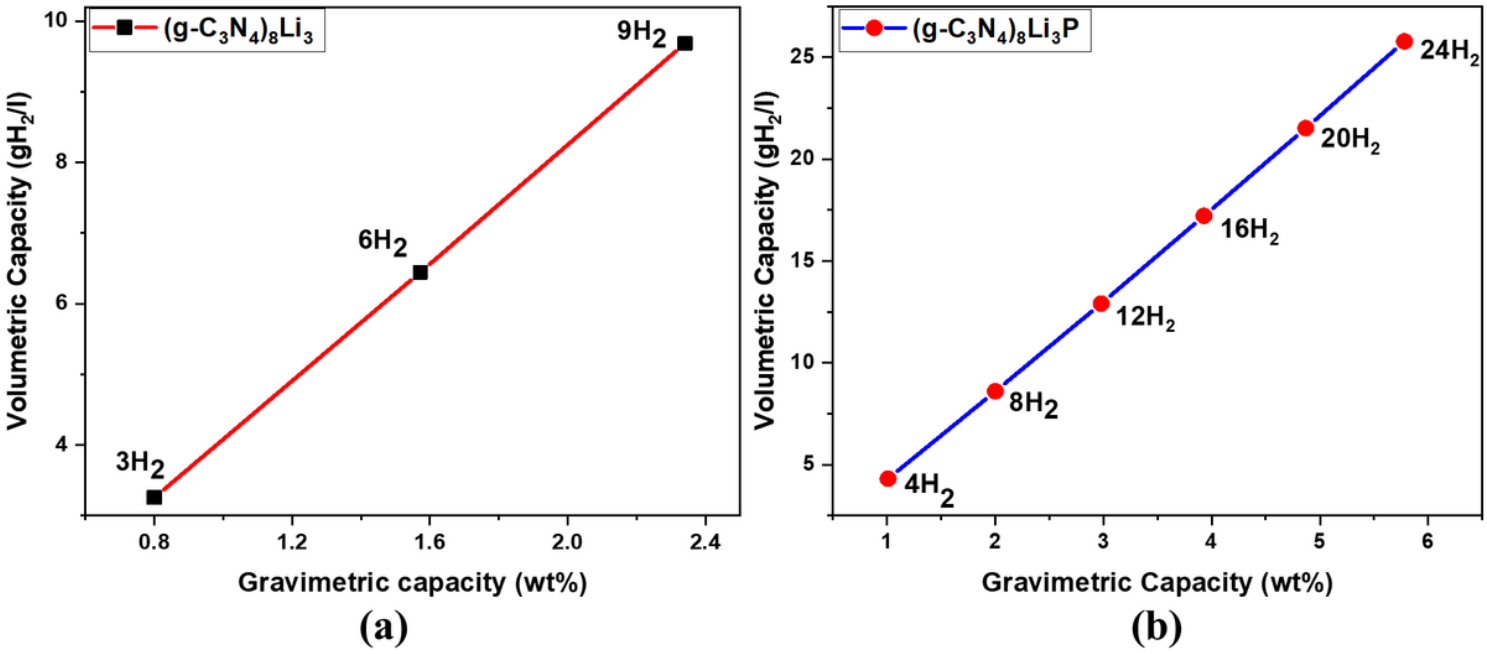

Figure 7

Volumetric capacity vs. gravimetric capacity plots of (a) $(g\text{-}C_3N_4)_8Li_3$ and (b) $(g\text{-}C_3N_4)_8Li_3P$ monolayers.

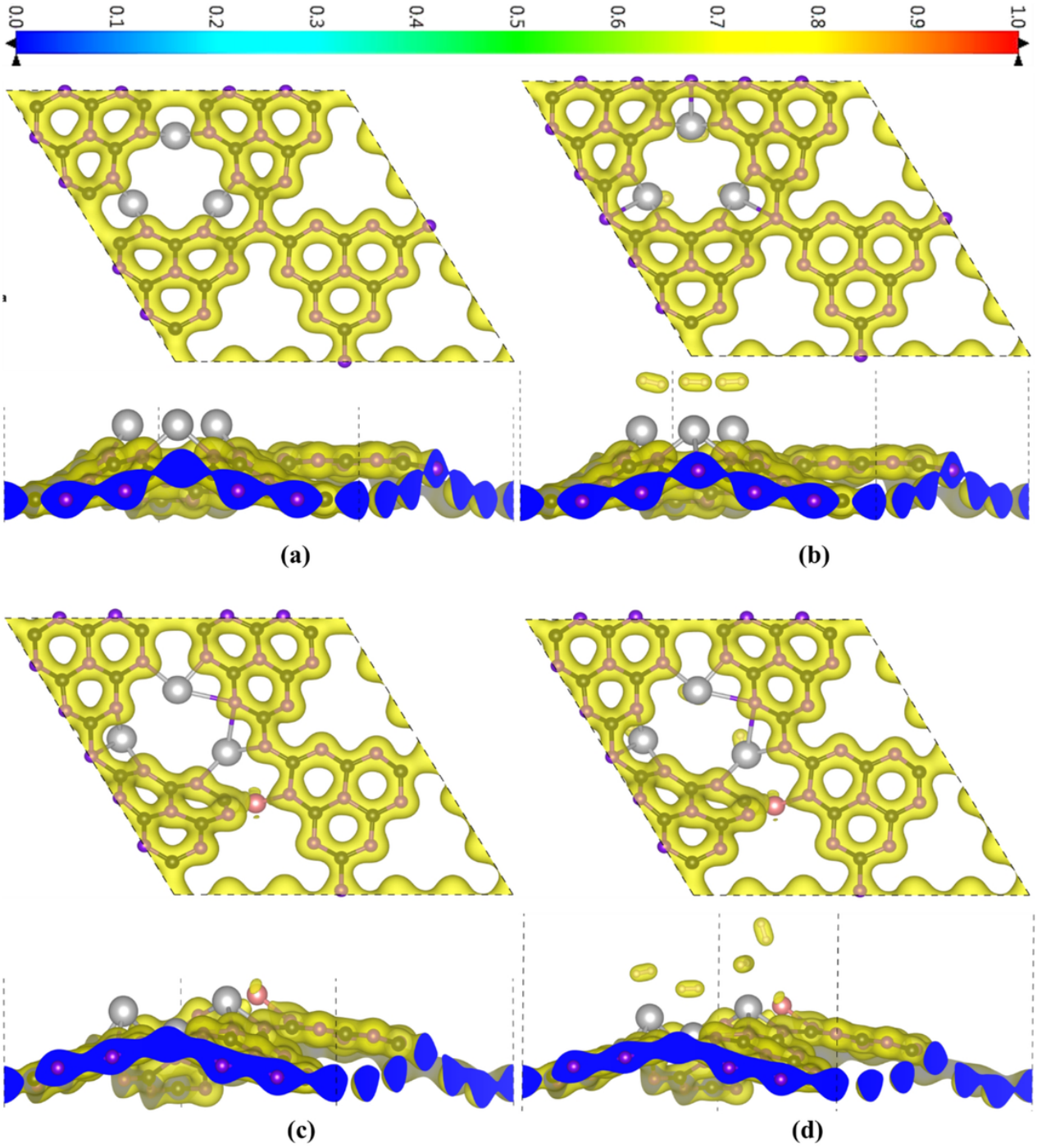

Figure 8

Total electron density plots for the system (a) $(g\text{-}C_3N_4)_8Li_3$, (b) $(g\text{-}C_3N_4)_8Li_3 + 3H_2$, (c) $(g\text{-}C_3N_4)_8Li_3P$, and (d) $(g\text{-}C_3N_4)_8Li_3P + 4H_2$. The isosurface value is taken as 0.02 e/Å^3.

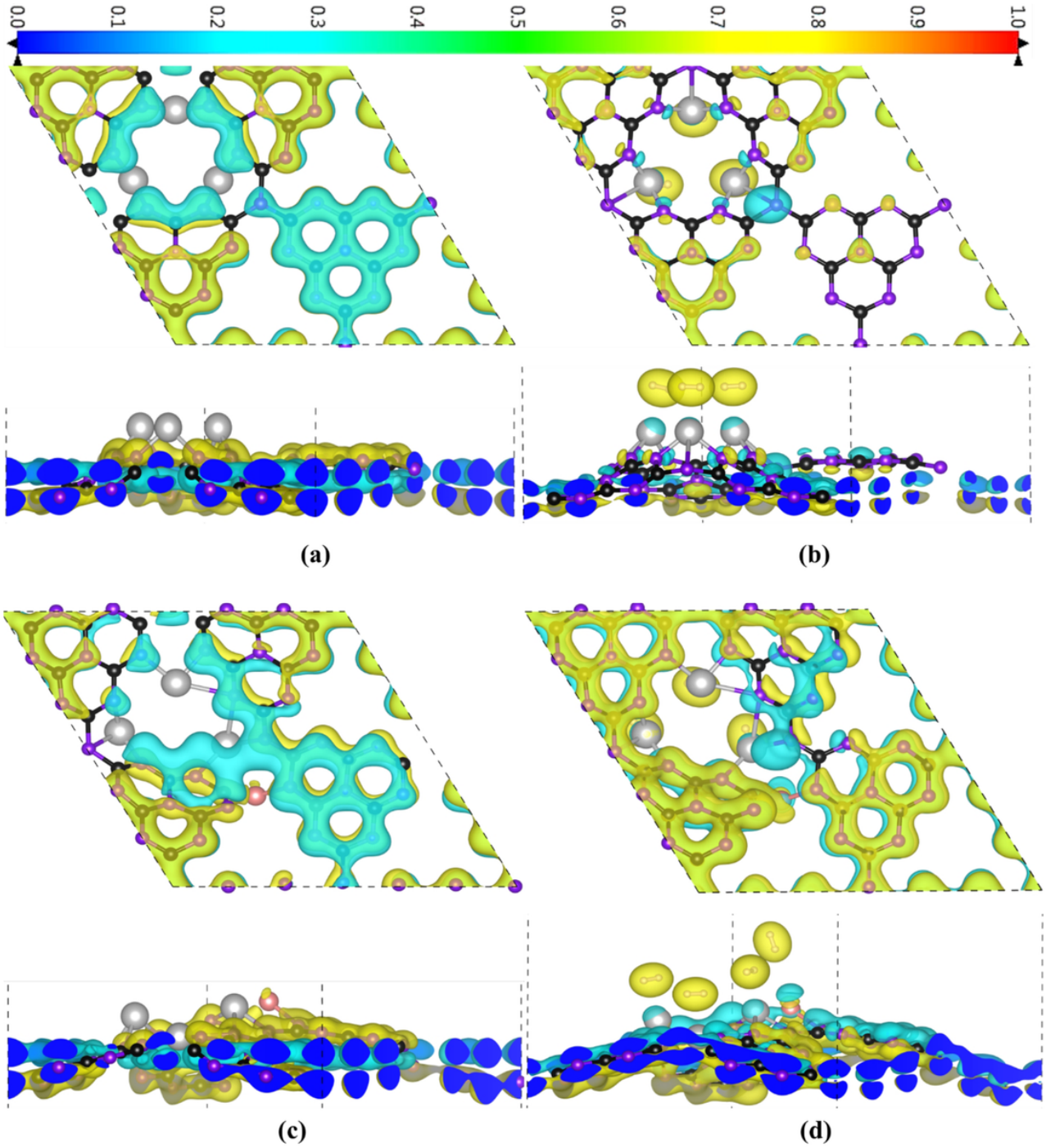

Figure 9

The charge density difference (CDD) plots for the system (a) $(g\text{-}C_3N_4)_8Li_3$, (b) $(g\text{-}C_3N_4)_8Li_3 + 3H_2$, (c) $(g\text{-}C_3N_4)_8Li_3P$, and (d) $(g\text{-}C_3N_4)_8Li_3P + 4H_2$. The isosurface value is taken as 0.02 e/Å^3. Charge depletion along accumulation is given by the light blue and yellow colors, respectively.

Supplementary Files

This is a list of supplementary files associated with this preprint. Click to download.

- Supplementaryinformationfile.docx